Available online at www.sciencedirect.com
ScienceDirect
Journal of Nuclear Materials 373 (2008) 199–205
journal of nuclear materials
www.elsevier.com/locate/jnucmat

Nature of defect clusters in neutron-irradiated iron-based alloys deduced from small-angle neutron scattering

F. Bergner [a,*], A. Ulbricht [a], A. Gokhman [b], D. Erak [c]

[a] Forschungszentrum Dresden-Rossendorf, Institute of Safety Research, P.O. Box 510119, 01314 Dresden, Germany
[b] South-Ukrainian Pedagogical University, UA-270020 Odessa, Ukraine
[c] RRC Kurchatov, Kurchatov Square 1, 123182 Moscow, Russia

Received 12 January 2007; accepted 23 May 2007

Abstract

Small-angle neutron scattering (SANS) was applied to investigate Fe-based model alloys with intentionally varied Cu levels. The aims are to provide size distributions of scatterers and to interpret deviations of the measured ratio of magnetic and nuclear scattering cross-sections from the ratios calculated for pure vacancy clusters and pure Cu clusters. For the case of the low-Cu alloy the SANS results indicate the average scatterer to be an Fe–Cu–vacancy cluster of about 1 nm radius, the composition of which is constricted according to given inequalities. For the case of the Cu-enriched alloy the SANS results are consistent with Cu-rich clusters of about 1.5 nm radius containing 15% vacancies per bcc lattice site.

1. Introduction

The nature of the nanometre-sized features responsible for the neutron-irradiation-induced degradation of the mechanical properties of reactor pressure vessel (RPV) steels is still subject to debate. This is because, firstly, there is a variety of nanoscale features of different types [1] and the factors influencing their relative importance are complex, and, secondly, the conclusions drawn from experimental investigations using different methods are partly in conflict with one another [2,3]. It is therefore helpful to study model alloys, where the diversity of nanoscale features is constricted due to composition and where dominant effects can be identified or even isolated.

The present approach is based on Fe-based model alloys with low-carbon and low nickel contents, similar levels of the solution hardeners Si and Mn as in Russian-type VVER RPV steels and intentionally varied Cu levels. Preliminary interpretation of the ratio of magnetic and nuclear SANS cross-sections (A-ratio) indicated the dominance of vacancy-rich clusters and Cu-rich clusters in the case of the low-Cu and Cu-enriched model alloys, respectively [4]. However, a more detailed consideration of the measured cross-sections revealed significant deviations between measured A-ratio and the value calculated for pure vacancy clusters or pure bcc Cu clusters.

The aim of the present paper is to interpret these deviations in detail taking into account the composition of the model alloys as well as the magnetic character of the Fe atoms in the clusters [5,6]. Furthermore, the results of complementary studies of the same model alloys [7] as well as similar materials [8] using positron annihilation spectroscopy (PAS) are exploited in the discussion.

2. Experiments

2.1. Materials and specimens

The materials investigated are low-carbon Fe-based model alloys with low (alloy A) or intentionally increased (alloy B) Cu such as to cover the range of impurity Cu of

* Corresponding author. Tel.: +49 351 260 3186; fax: +49 351 260 2205.
E-mail address: F.Bergner@fzd.de (F. Bergner).

0022-3115/$ - see front matter © 2007 Elsevier B.V. All rights reserved.
doi:10.1016/j.jnucmat.2007.05.044

Table 1
Composition of the model alloys (in wt%, balance Fe)

Material	C	Si	Mn	S	P	Ni	Cu
A	0.01	0.15	0.39	0.04	0.002	0.01	0.015
B	0.01	0.24	0.49	0.05	0.012	0.01	0.42

Table 2
Irradiation conditions applied to alloys A and B

Irradiation condition	Irradiation temperature/ °C	Neutron fluence ($E > 0.5$ MeV)/ 10^{18} cm^{-2}	Neutron flux ($E > 0.5$ MeV)/ 10^{12} cm^{-2} s^{-1}
A1, B1	270	10 (≈0.01 dpa)	0.4
A2, B2	270	80 (≈0.08 dpa)	3.0

RPV steels of first and later generation RPVs. The composition of the model alloys is given in Table 1. The solute elements Mn and Si are similar as in VVER-type RPV steels, whereas Ni is essentially absent.

Charpy specimens of alloys A and B were irradiated with neutrons at surveillance positions of the VVER440 reactors ROVNO1 and KOLA3 over one reactor cycle. The irradiation conditions denoted 1 and 2, respectively, are specified in Table 2.

From the undeformed part of broken Charpy specimens several slices of about 1 mm thickness were machined for the purpose of SANS and hardness measurements in the unirradiated, as-irradiated or irradiated and annealed condition. Post-irradiation annealing was performed at 475 °C/100 h, i.e. about the condition of large-scale anneals performed for VVER440 RPVs.

2.2. Measurements

The SANS experiment was carried out at the BENSC V4 spectrometer at Hahn-Meitner-Institut (HMI) Berlin. The SANS instrument, V4, and the data processing software, BerSANS-PC, were described in detail in [9] and [10], respectively. Neutron wavelength was 0.6 nm. A two-dimensional position-sensitive detector was placed at distances of 1.1 m and 4 m from the specimen in order to cover a range of scattering vectors, Q, from about 0.1 to 3 nm^{-1}. Background correction and absolute calibration using a water standard were performed. A saturation magnetic field of 1.2 T oriented perpendicular to the neutron beam direction was applied to the specimens. This allows for the separation of the nuclear and magnetic contributions from the total scattered intensity. Part of the results was tentatively reported immediately after the SANS experiment [4]. Since then, analysis has been significantly refined and results from positron annihilation Doppler broadening and lifetime measurements for the same materials have become available [7].

A number of 10 Vickers hardness tests with load, $F = 98.1$ N, were performed for each material condition in order to derive estimates of the mean value and standard deviation of Vickers hardness, HV10.

3. Experimental results

The nuclear and magnetic scattering cross-sections measured for the model alloys A and B are summarized in Figs. 1 and 2.

For model alloy A an irradiation-induced increase of the scattering cross-section is observed at higher values of the scattering vector, Q. The Q value of first deviation from the unirradiated reference is equal for the magnetic cross-sections of conditions A1 and A2, $Q > 0.5$ nm^{-1}, but slightly differs for the nuclear cross-section. The excess scattering for the irradiated conditions is an increasing function of neutron fluence. For condition A1 this contribution completely disappears on average after annealing at 475 °C for 10 h. However, the relative scatter of the data obtained at high Q values/low intensities is large and no further data processing was performed for the annealed condition of alloy A1.

For model alloy B there is an irradiation-induced increase of the scattering cross-section starting at a slightly smaller Q value, $Q > 0.3$ nm^{-1}, than for alloy A. An increase of the neutron fluence from 0.01 dpa to 0.08 dpa does not further raise the scattering cross-section. In contrast with alloy A1 the irradiation-induced scattering cross-section of alloy B1 does not disappear after annealing but the Q range is shifted to lower values.

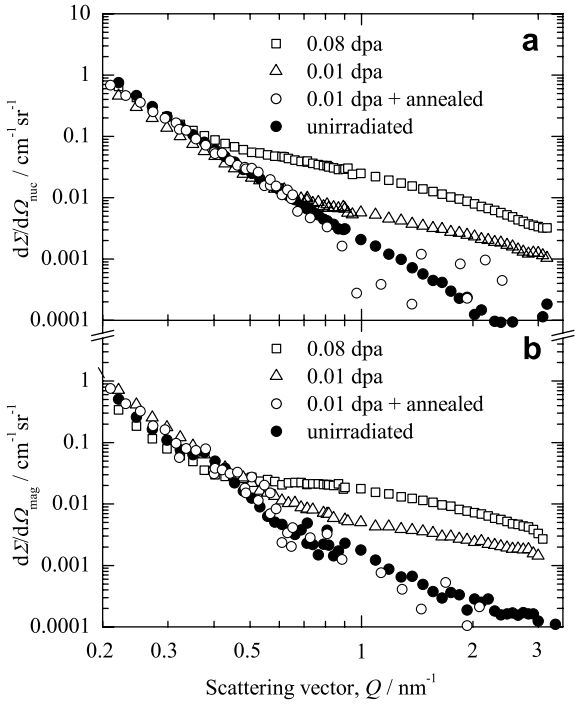

Fig. 1. Coherent nuclear (a) and magnetic (b) scattering cross-sections of iron alloy A for the unirradiated condition, two irradiated conditions distinguished by the respective neutron fluences in units of dpa and a post-irradiation annealed condition.

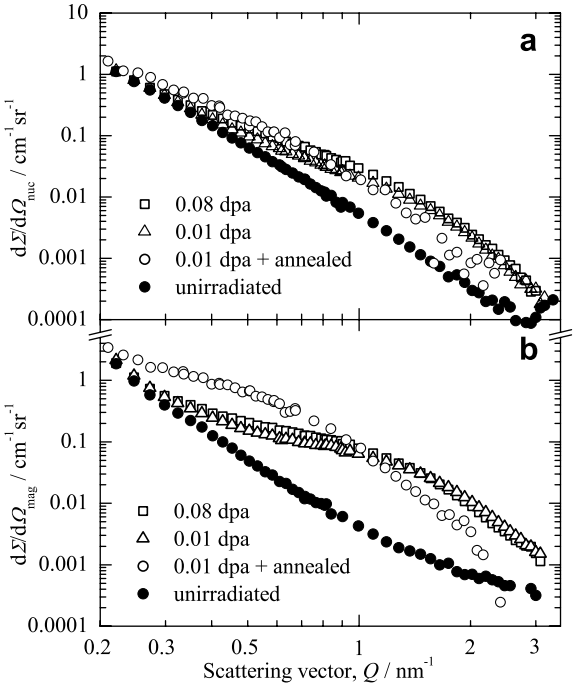

Fig. 2. Coherent nuclear (a) and magnetic (b) scattering cross-sections of iron alloy B for the unirradiated condition, two irradiated conditions distinguished by the respective neutron fluences in units of dpa and a post-irradiation annealed condition (475 °C/100 h).

These findings can be discussed in more detail, if the size distribution of irradiation-induced scatterers is considered. In general, the size distribution (here volume fraction, c_R, per size class) can be obtained by Fourier transformation from either the magnetic or the nuclear scattering cross-section, Eq. (1). As long as the magnetic and nuclear scattering contrast, $\Delta\eta^2$, is unknown, the size distribution is obtained in relative units only

$$\frac{d\Sigma}{d\Omega}(Q) \rightarrow c_R \Delta\eta^2(R). \quad (1)$$

In the present case, the size distribution of scatterers was calculated according to [11] on the assumption of homogeneous non-magnetic spherical scatterers dispersed in a homogeneous matrix. For non-magnetic scatterers the magnetic contrast is equal to the square of the magnetic scattering length of Fe and absolute values of the volume fraction of scatterers can be calculated according to Eq. (2)

$$c_R = \frac{(c_R \Delta\eta^2)_{mag,measured}}{\Delta\eta^2_{mag}}. \quad (2)$$

The volume-related size distribution is shown in Figs. 3 and 4. The annealed condition of alloy A was not included in the analysis because of large data scatter. However, any remaining total volume fraction of irradiation-induced scatterers must be much less than for conditions A1 and A2. The assumption of non-magnetic scatterers will be reconsidered in the discussion section.

The characteristics of the irradiation-induced defect/solute atom clusters are listed in Table 3. Only clusters larger

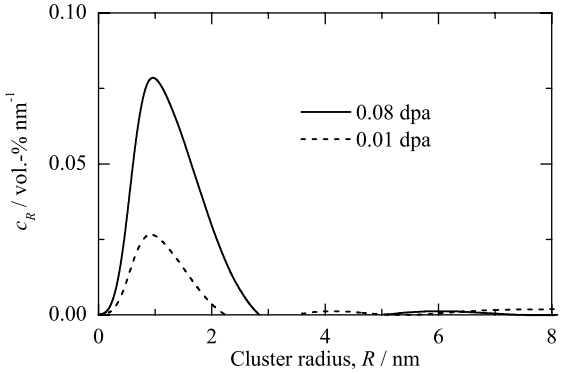

Fig. 3. Volume fraction of non-magnetic irradiation-induced clusters per radius interval of iron alloy A for two irradiation conditions, calculated from the data of Fig. 1(b), unirradiated condition subtracted.

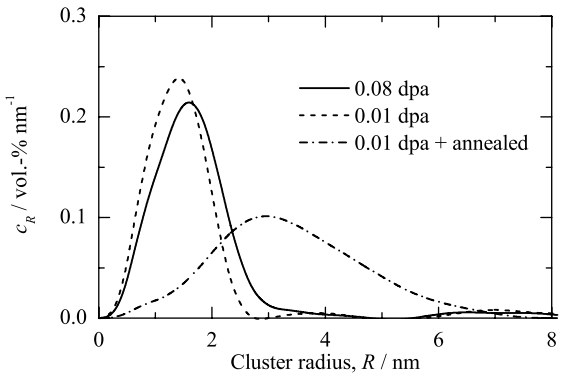

Fig. 4. Volume fraction of non-magnetic irradiation-induced clusters per radius interval of iron alloy B for two irradiation conditions and a post-irradiation annealing (475°C/100 h), calculated from the data of Fig. 2(b), unirradiated condition subtracted.

Table 3
Distribution parameters of irradiation-induced clusters. Apparent values of volume fraction and number density derived from magnetic SANS contribution assuming non-magnetic scatterers

Material/condition	Apparent total volume fraction/%	Peak radius/nm	Apparent total number density/cm^{-3}	A-ratio
A1	0.027 ± 0.005	0.93 ± 0.10	0.4×10^{17}	1.7 ± 0.1
A2	0.099 ± 0.010	0.96 ± 0.10	1.3×10^{17}	1.7 ± 0.1
B1	0.303 ± 0.010	1.46 ± 0.10	2.9×10^{17}	5.3 ± 0.3
B2	0.307 ± 0.010	1.61 ± 0.10	2.2×10^{17}	5.0 ± 0.3

than the detection limit of SANS ($R > 0.5$ nm under the present conditions) were taken into account in the calculation of total volume fractions and number densities.

The A-ratio originally defined as ratio of the scattering cross-sections, $d\Sigma/d\Omega$, perpendicular and parallel to the magnetic field direction [12] was calculated according to Eq. (3) from the measured size distributions, c_R, of irradiation-induced scatterers scaled with the (a priori unknown) magnetic (mag) and nuclear (nuc) scattering contrast, $\Delta\eta^2_{mag}$ and $\Delta\eta^2_{nuc}$, respectively. In general, the magnetic

Table 4
Measured values of Vickers hardness, HV10

Irradiation condition	Vickers hardness, HV10	
	Model alloy A	Model alloy B
Unirradiated reference	110	136
Irradiated, 0.01 dpa	204	202
Irradiated, 0.08 dpa	233	215
Irradiated and annealed, 475 °C/100 h	107	158

and nuclear scattering contrasts are different functions of radius, R. In order to obtain a robust average value of the A-ratio, the size distributions were integrated over R

$$A = \frac{(\mathrm{d}\Sigma/\mathrm{d}\Omega)_{\perp}}{(\mathrm{d}\Sigma/\mathrm{d}\Omega)_{\parallel}} = \frac{(\mathrm{d}\Sigma/\mathrm{d}\Omega)_{\mathrm{mag}}}{(\mathrm{d}\Sigma/\mathrm{d}\Omega)_{\mathrm{nuc}}} + 1 = \frac{\int c_{\mathrm{R}} \Delta\eta^2_{\mathrm{mag}} \mathrm{d}R}{\int c_{\mathrm{R}} \Delta\eta^2_{\mathrm{nuc}} \mathrm{d}R} + 1. \quad (3)$$

The mean values of the measured Vickers hardness, HV10, are listed in Table 4.

4. Discussion

4.1. General considerations

The size distributions observed in the present work may be characterized as single-peaked. Note that our analysis is basically capable of detecting the superposition of distinctive distributions centred at different sizes. In the following analysis we repeatedly refer to the concept of an 'average' cluster defined as a cluster composed according to the average composition of all irradiation-induced clusters in the probed volume of some 10 mm^3. The effect of any internal structure of individual clusters (for instance core-shell structure [13]) is incorporated in the concept of an average cluster introduced above. This approach has been justified by reference to scattering theory [14].

For the case of a two-phase matrix-inclusion microstructure with a homogeneous pure bcc Fe matrix and with independent inclusions (defect/atom clusters specified as average clusters), which are fully coherent with the bcc Fe matrix, the contrast (magnetic or nuclear) assumes the following special form:

$$\Delta\eta^2 = \left(\sum_{X\in\mathrm{cluster}} n^{\mathrm{C}}_X b^{\mathrm{C}}_X - \sum_{X\in\mathrm{matrix}} n^{\mathrm{M}}_X b^{\mathrm{M}}_X \right)^2 = \left(\sum_{X\in\mathrm{cluster}} n^{\mathrm{C}}_X b^{\mathrm{C}}_X - b^{\mathrm{M}}_{\mathrm{Fe}} \right)^2, \quad (4)$$

b_X is the magnetic or nuclear scattering length of element X (including vacancies, $X = v$), n_X is the fraction of element X per regular bcc lattice sites and superscripts C and M refer to cluster and matrix, respectively. After applying the magnetic and nuclear contrast defined in Eq. (4) to Eq. (3) the following expression for the A-ratio is obtained:

$$A = 1 + \left[\frac{\left(\sum_{X\in\mathrm{cluster}} n^{\mathrm{C}}_X b^{\mathrm{C}}_X - b^{\mathrm{M}}_{\mathrm{Fe}}\right)_{\mathrm{mag}}}{\left(\sum_{X\in\mathrm{cluster}} n^{\mathrm{C}}_X b^{\mathrm{C}}_X - b^{\mathrm{M}}_{\mathrm{Fe}}\right)_{\mathrm{nuc}}} \right]^2 = 1 + \left(\frac{n^{\mathrm{C}}_{\mathrm{Fe}} b^{\mathrm{C}}_{\mathrm{mag,Fe}} - b^{\mathrm{M}}_{\mathrm{mag,Fe}}}{\sum_{X\in\mathrm{cluster}} n^{\mathrm{C}}_X b_{\mathrm{nuc},X} - b_{\mathrm{nuc,Fe}}} \right)^2. \quad (5)$$

Let us first consider vacancy clusters and diluted zones consisting of Fe atoms (with $b^{\mathrm{C}}_{\mathrm{mag,Fe}} = b^{\mathrm{M}}_{\mathrm{mag,Fe}} = 6.0$fm, $b^{\mathrm{C}}_{\mathrm{nuc,Fe}} = b^{\mathrm{M}}_{\mathrm{nuc,Fe}} = 9.45$ fm) and vacancies only. Then Eq. (5) reduces to:

$$A = 1 + \left[\frac{6.0 \cdot (n^{\mathrm{C}}_{\mathrm{Fe}} - 1)}{9.45 \cdot (n^{\mathrm{C}}_{\mathrm{Fe}} - 1)} \right]^2 = 1.40. \quad (6)$$

The same result, $A = 1.40$, also holds for planar clusters of self-interstitial atoms (SIA) or vacancies, i.e. dislocation loops as the stable configuration in the size range of interest. However, dislocation loops cannot account for the observed scattering cross-sections, as shown by direct application of scattering theory [15] taking into account a realistic estimation by means of TEM of number densities of dislocation loops in RPV steels, $N \approx 10^{16}\,\mathrm{cm}^{-3}$, and model alloys under similar irradiation conditions [16]. It is emphasized that we do not claim the absence of dislocation loops.

Comparison of the A-ratio calculated for vacancy-type clusters, $A = 1.40$, with the measured values, $A = 1.7$ for alloy A and $A = 5.0 \ldots 5.3$ for alloy B, shows that the average cluster detected by SANS is not a pure vacancy-type cluster in both cases. In other words, the average cluster must contain additional elements, Cu, Mn or Si in particular (see Table 1). The effect of Cu, which is known to be highly enriched in irradiation-induced clusters in RPV steels, is considered first, separately for the low-copper alloy A and the Cu-enriched alloy B. Other elements will be discussed subsequently.

Cu atoms are slightly larger than Fe atoms. We exclude Cu atoms on interstitial sites of the bcc lattice [17] as well as clusters simultaneously containing Cu atoms and SIAs [18] and restrict ourselves to clusters composed of Cu and Fe atoms on regular lattice sites and vacancies. If coherency strain is neglected, Eq. (5) reduces to the following expressions:

$$A = 1 + \left[\frac{b^{\mathrm{C}}_{\mathrm{mag,Fe}} \cdot n^{\mathrm{C}}_{\mathrm{Fe}} - 6.0}{9.45 \cdot (n^{\mathrm{C}}_{\mathrm{Fe}} - 1) + 7.72 \cdot n^{\mathrm{C}}_{\mathrm{Cu}}} \right]^2, \quad (7)$$

$$n_{\mathrm{v}} = 1 - (n^{\mathrm{C}}_{\mathrm{Fe}} + n^{\mathrm{C}}_{\mathrm{Cu}}). \quad (8)$$

4.2. Low-copper alloy

The question to be answered is, whether the deviation of the measured value of the A-ratio, $A = 1.7 \pm 0.1$, from the value, $A = 1.40$, calculated for clusters of self-defects according to Eq. (5) may be caused by Cu in the case of model alloy A, conditions A1 and A2. The equal values

of the A-ratio (Table 3) indicate the same type of scatterer for both conditions. Fe-free Cu–vacancy clusters are not a possible candidate of the average cluster, because the required minimum Cu content of the alloy according to Eqs. (7) and (8) is 0.029 at.% (or 0.033 wt%), i.e. more than double the available Cu of 0.015 wt%. Therefore, we have to focus on ternary Fe–Cu–vacancy clusters. The magnetic scattering length of Fe in a mixed nm-sized cluster is not known in advance. Two extreme cases are separately considered below.

(a) $b^{C}_{mag,Fe} = 0$.

In this case the assumption of non-magnetic scatterers is applicable. Due to both the Cu content of alloy A and the measured volume fraction of clusters for condition A2 the maximum possible Cu fraction in the average cluster is $n_{Cu} = 0.13$. This requires $n_{Fe} = 0.135$ and $n_v = 0.735$ according to Eqs. (7) and (8) in order to obtain the observed value of A. Further analysis shows that the cluster compositions compatible with the full set of measurements for alloy A, condition A2 must be in the range given by Eq. (9):

$$0 < n^{C}_{Cu} < 0.13, \quad n^{C}_{Fe} + n^{C}_{Cu} = 0.25 \pm 0.015, \quad n_v = 0.75 \pm 0.015. \tag{9}$$

The measurements performed do not allow for the distinction of Cu fractions between these limits. Eq. (9) also applies to irradiation condition A1, but the upper limit of the allowed Cu fraction of the average cluster is shifted to higher values because of the lower volume fraction of clusters. However, it would be unreasonable to assume different compositions of clusters in the same material irradiated at different neutron fluxes (same temperature and time) at least in the present low-flux range (0.01–0.08 displacements per atom).

Regarding the morphology of an average cluster according to Eq. (9), it is important to note that a vacancy fraction of 0.75 is well beyond any typical macroscopic percolation limit. For instance, the self-consistent approach to effective elasticity [19] yields a critical concentration for zero effective moduli of 0.5 for a solid with pores. It is therefore impossible to build the average cluster as a superposition of compact individual clusters of uniform composition (as opposed to a shell structure with vacancies confined to the core). About 50% of the volume of a spherical cluster of 1 nm radius (about the peak radius observed by SANS, see Table 3) is located in a distance from the matrix interface shorter than the nearest-neighbour distance of the bcc lattice. In other words, all the Cu and Fe atoms are expected to form an incomplete one-atomic layer at the cluster–matrix interface. This type of shell structure was concluded to be the stable configuration in pure Cu–vacancy clusters [20]. However, Fe atoms in contact with the Fe matrix and at a Cu/Fe ratio in the shell, n^{C}_{Cu}/n^{C}_{Fe}, less than or about 1 should bear a magnetic moment [5]. This conclusion is in conflict with the assumption made before, i.e. the assumption (a) has to be rejected.

(b) $b^{C}_{mag,Fe} = b^{M}_{mag,Fe} = 6.0$nm.

In this case, the volume fractions listed in Table 3 have to be corrected in order to take into account the resulting magnetic character of the clusters. The correction factor is $(1 - n^{C}_{Fe})^2$, i.e. it depends on Fe fraction. The condition of maximum available Cu of 0.013 at.% and the measured A-ratio, $A = 1.7$, constrict the possible cluster compositions to the range according to Eq. (10). The measurements performed do not allow for the distinction of Cu fractions between the limits.

$$0 < n^{C}_{Cu} < 0.225, \quad n^{C}_{Fe} = 1 - 3.39 n^{C}_{Cu}, \quad n_v = 2.39 n^{C}_{Cu}. \tag{10}$$

Regarding the magnetic character of the Fe atoms in an average cluster, the Cu/Fe ratio according to Eq. (10) is always significantly less than 1, i.e. there is no conflict with the assumption on the magnetic character of the Fe atoms belonging to the cluster [5]. The vacancy fraction according to Eq. (10) is less than 0.45, i.e. less than the percolation limit mentioned above. It is therefore possible to construct an average Fe–Cu–vacancy cluster of uniform composition (as opposed to shell structure) according to Eq. (10).

It is instructive to refer to a positron annihilation study of the same alloy A at this point [7]. In that study small vacancy (open volume type) clusters of about 2–6 vacancies were reported on the basis of positron lifetime measurements. This conclusion is incompatible with the high vacancy fraction, $n_v = 0.75$, deduced for case (a), but it does not conflict with case (b). In particular, a Fe–Cu–vacancy cluster of 1 nm size can be an agglomeration of several small vacancy clusters consisting of 2–6 vacancies each and separated from each other by a distribution of Fe and Cu atoms. Case (b) is also consistent with the results of a positron annihilation study of a neutron-irradiated Fe–0.05 wt% Cu model alloy [8], according to which agglomerations of vacancies and Cu atoms were clearly identified. Uncollapsed agglomerations of small vacancy clusters were identified in computer simulations of the cascade stage [21].

Consequently, case (b) is favoured over case (a). The initially posed question has to be affirmed: The deviation of the measured value of the A-ratio from the value, $A = 1.40$, can be explained by the contribution of Cu (besides Fe and vacancies) in the case of model alloy A, conditions A1 and A2. Based on the application of Eq. (5), secondary influence factors are evaluated as follows:

- The addition of Mn to any cluster of self-defects would lower (not raise as observed) the A-ratio because of the negative nuclear scattering length. Therefore, Mn cannot explain the observed A-ratio.
- In principle, the addition of Si can explain the observed A-ratio. The minimum required Si fraction is $n^{C}_{Si} = 0.32$. This fraction corresponds to an enrichment factor of Si in clusters relative to matrix Si of about 100, which is much beyond the enrichment factors (about 4) typically observed for RPV steels or model alloys of similar Si levels [22].

- The effects of Si and Mn in proportion approximately cancel out because of the scattering lengths of opposite sign.
- The strain fields of vacancies and oversized Cu atoms are expected to cancel out at least partly. Therefore, the influence of strain should be rather unimportant.

In conclusion, the favoured cluster configuration for alloy A is Cu–Fe–vacancy clusters with uniform composition according to Eq. (10) and with Fe atoms exhibiting a magnetic moment. Enrichment with Mn and Si with $n^{C}_{Si} \geqslant n^{C}_{Mn}$ is not excluded. This configuration can essentially be identified with vacancy–solute atmospheres [1,8,23].

4.3. Fe–0.42 wt% Cu alloy

Because of both increased Cu content of model alloy B and existing experience on Cu-enriched Fe and RPV steels [2,24] it is reasonable to assume the formation of Cu-rich clusters (also called precipitates). In particular, consistency of pure Cu clusters or Cu–vacancy clusters with the experimental findings will be checked below.

Pure Cu clusters in the size range observed are known to be coherent with the bcc Fe lattice [25]. Due to the larger atom size of Cu relative to Fe ($r_{Cu} = 0.1278$ nm, $r_{Fe} = 0.1241$ nm) the lattice is distorted [26]. Taking the misfit parameter, $r_{Cu}/r_{Fe} - 1 = 0.030$, as an upper limit of the distortion, the A-ratio is obtained to be in the range, $7.37 < A < 13.0$. This range still significantly deviates from the measured A-ratio, $A = 5.0$ to $A = 5.3$. It can be concluded that the average irradiation-induced scatterer is not a pure bcc Cu cluster. This conclusion is in agreement with previous results [27]. Furthermore, the analysis [27] also indicates that the average scatterer is different from a bcc Cu–Fe cluster.

Cu–vacancy clusters are considered next. Coherency strain is less important because the effects of oversized Cu and vacancies cancel out at least partly. If strain is ignored, vacancy fractions of Cu–vacancy clusters of 0.165 and 0.150 are required for irradiation conditions B1 and B2 of model alloy B, respectively, in order to reproduce the measured A-ratios. The observed composition is supported by reference to the formation mechanism, because Cu atoms require vacancies to be transported to a cluster under the present conditions and there is a positive binding energy of an accompanying vacancy to a Cu cluster or Cu–vacancy cluster [20]. It is also consistent with both the irradiation-induced increase of the mean positron lifetime observed for the same alloy [7] and PAS results reported for a pure Fe–0.3 wt% Cu alloy [8].

4.4. Cluster fraction and hardness

In Section 4.2 the range of possible compositions of irradiation-induced clusters was specified as much as possible. A consequence of the remaining ambiguity for the case of model alloy A is that the evaluated volume fractions of clusters depend on assumptions on both fraction and magnetic moment of Fe in the clusters. The volume fractions and number densities given in Table 3 for alloy A have, therefore, to be interpreted as lower bounds and cannot be definitely specified.

Although the value of the Vickers hardness for the unirradiated condition of the Cu-enriched alloy B is higher than for alloy A, the hardness values for the irradiated conditions essentially agree. It can be concluded that the effect of irradiation-induced vacancy-rich defects on Vickers hardness is dominant in comparison with that of Cu-bearing precipitates in the present case.

Annealing gives rise to a recovery of the hardness to the unirradiated reference in the case of model alloy A, whereas the initial hardness is not fully recovered for model alloy B. This is consistent with the observed cluster dissolution and the cluster coarsening for model alloys A and B, respectively.

5. Conclusions

For a low-Cu (0.015 wt% Cu) Fe-based model alloy the average irradiation-induced cluster detected by SANS is suggested to be essentially Fe–Cu–vacancy clusters characterized by

- peak radius of 0.93–0.96 nm, maximum radius of 2.2–2.8 nm and lower bound number density of 0.4–1.3×10^{17} cm^{-3} in the covered fluence range,
- the range of possible compositions according to Eq. (10),
- Fe atoms bearing a magnetic moment,
- agglomerations of up to 6 vacancies uniformly distributed inside the clusters.

Minor enrichments of Mn and Si cannot be excluded.

For a Cu-enriched (0.42 wt% Cu) Fe-based model alloy the SANS results can be entirely explained by Cu clusters containing about 0.15 vacancies per bcc lattice site. Some Fe atoms in the non-magnetic state cannot be excluded. Peak radius slightly increases from 1.46 to 1.61 nm and number density slightly decreases from 3 to 2.2×10^{17} cm^{-3} in the covered fluence range. Annealing at 475 °C/100 h gives rise to dissolution in the case of the low-Cu alloy and to coarsening in the case of the Cu-enriched alloy.

Acknowledgements

The work was partially funded by the EU within the integrated project PERFECT. The SANS experiment was carried out at the BENSC V4 spectrometer at Hahn-Meitner-Institut Berlin. Assistance of P. Strunz is gratefully acknowledged.

References

[1] G.R. Odette, B.D. Wirth, J. Nucl. Mater. 251 (1997) 157.
[2] M.K. Miller, B.D. Wirth, G.R. Odette, Mater. Sci. Eng. A 353 (2003) 133.
[3] A. Ulbricht, F. Bergner, J. Böhmert, M. Valo, M.-H. Mathon, A. Heinemann, Philos. Mag. 87 (2007) 1855.
[4] A. Ulbricht, J. Böhmert, M. Grosse, P. Strunz, Physica B 276–278 (2000) 936.
[5] K. Sumiyama, T. Yoshitake, Y. Nakamura, J. Phys. Soc. Jpn. 53 (1984) 3160.
[6] P. Asoka-Kumar, B.D. Wirth, P.A. Sterne, R.H. Howell, G.R. Odette, Philos. Mag. Lett. 82 (2002) 609.
[7] S.E. Cumblidge, A.T. Motta, G.L. Catchen, G. Brauer, J. Böhmert, J. Nucl. Mater. 320 (2003) 245.
[8] Y. Nagai, Z. Tang, M. Hassegawa, T. Kanai, M. Saneyasu, Phys. Rev. B 63 (2001) 134110.
[9] U. Keiderling, A. Wiedenmann, Physica B 213&214 (1995) 895.
[10] U. Keiderling, Appl. Phys. A 74 (Suppl.) (2002) S1455.
[11] O. Glatter, J. Appl. Cryst. 13 (1980) 7.
[12] G. Solt, F. Frisius, W.B. Waeber, P. Tipping, in: A.S. Kumar, D.S. Gelles, R.K. Nanstadt, E.A. Little (Eds.), Effects of Radiation on Materials: 16th Int. Symp., ASTM STP 1175, ASTM, Philadelphia, 1993, p. 444.
[13] M. Große, A. Gokhman, J. Boehmert, Nucl. Instrum. and Meth. B 160 (2000) 515.
[14] A. Gokhman, J. Boehmert, A. Ulbricht, J. Nucl. Mater. 334 (2004) 195.
[15] A. Seeger, M. Rühle, Ann. Physik 11 (1963) 216.
[16] E.A. Kuleshova, B.A. Gurovich, Ya.I. Shtrombakh, D.Yu. Erak, O.V. Lavrenchuk, J. Nucl. Mater. 300 (2002) 127.
[17] G.J. Ackland, D.J. Bacon, A.F. Calder, T. Harry, Philos. Mag. A 75 (1997) 713.
[18] F. Maury, A. Lucasson, P. Lucasson, P. Moser, F. Faudot, J. Phys.: Condens. Matter 2 (1990) 9291.
[19] R. Hill, J. Mech. Phys. Solids 13 (1965) 213.
[20] A. Takahashi, N. Soneda, S. Ishino, G. Yagawa, Phys. Rev. B 67 (2003) 024104.
[21] R.E. Stoller, J. Nucl. Mater. 276 (2000) 22.
[22] P. Auger, P. Pareige, S. Welzel, J.-C. Van Duysen, J. Nucl. Mater. 280 (2000) 331.
[23] P. Auger, P. Pareige, M. Akamatsu, D. Blavette, J. Nucl. Mater. 225 (1995) 225.
[24] G.R. Odette, Scripta Metall. 17 (1983) 1183.
[25] P.J. Othen, M.L. Jenkins, G.W. Smith, Philos. Mag. A 70 (1994) 1.
[26] Yu.N. Osetsky, A. Serra, Philos. Mag. A 73 (1996) 249.
[27] M.H. Mathon, A. Barbu, F. Dunstetter, F. Maury, N. Lorenzelli, C.H. de Novion, J. Nucl. Mater. 245 (1997) 224.